Crack-Initiation Toughness and Crack-Arrest Toughness in Advanced 9 Pct Ni Steel Welds Containing Local Brittle Zones

JAE-IL JANG, BAIK-WOO LEE, JANG-BOG JU, DONGIL KWON, and WOO-SIK KIM

The present study investigates the influence of local brittle zones (LBZs) on the fracture resistance of the heat-affected zones (HAZs) in quenched, lamellarized, and tempered (QLT) 9 pct Ni steel weld joints. The results of Charpy impact tests using simulated coarse-grained, heat-affected zone (CGHAZ) specimens show that the intercritically reheated (IC) CGHAZ and unaltered (UA) CGHAZ are the primary and secondary LBZs, respectively, of the steel at cryogenic temperature. Compact crack arrest (CCA) tests and crack-tip opening displacement (CTOD) tests were conducted at a liquefied natural gas (LNG) temperature to measure the variations in crack-arrest toughness and crack-initiation toughness along the distance from the fusion line (FL) within the actual HAZ. While CTOD tests show a decrease in toughness when approaching the FL, *i.e.*, the regions containing LBZs, the crack-arrest-toughness values are found to be higher than those in the regions near the base materials. This is due to the fact that the crack-arrest toughness is governed by the fraction of microstructures surrounding LBZs instead of the LBZs themselves. By direct comparison of the brittle-crack-arrest toughness (K_a) with the brittle-crack-initiation toughness (K_c), this investigation has determined that, with regard to crack-arrest behavior, the LBZs of QLT-9 pct Ni steel do not limit the practical safety performance of the weld joints in LNG storage tanks.

I. INTRODUCTION

NATURAL gas is expected to be one of this century's most important energy sources, because it provides clean energy with a high energy density, and, thus, the global demand for liquefied natural gas (LNG) has been increasing continuously. Because LNG is stored at or below its boiling temperature (111 K), the inner walls of LNG storage tanks must be constructed with a material which possesses high strength and suitable fracture toughness at cryogenic temperatures. The 9 pct Ni steel has been widely used for the construction of the inner walls, because of its excellent fracture toughness at the LNG temperature. Recently, in response to increasing demand for large-scale LNG storage tanks, advanced 9 pct Ni steels exhibiting a higher cryogenic toughness have been developed. One of these newly developed cryogenic steels is a quenched, lamellarized, and tempered (QLT) 9 pct Ni steel now used for LNG storage tanks in Korea.[1,2] The QLT process, originally developed for lower-Ni steel such as 5.5 pct Ni steel,[3] enhances cryogenic toughness considerably compared to other conventional processes, such as quenching and tempering or double-normalizing and tempering, due to the increased amount of stable austenite and the refinement of the effective grain size.

During the construction of LNG storage tanks, however, the excellent cryogenic fracture performance of QLT-9 pct Ni steel can be upset in the heat-affected zones (HAZs) near the fusion line (FL) by welding thermal cycles that can produce small areas, called local brittle zones (LBZs), which exhibit abnormally poor fracture resistance. Many studies on the influence of LBZs on the fracture performance of the welds have shown that LBZs cause low toughness values in multipass welded structural steel in various toughness tests, such as the Charpy impact test and the crack-tip opening displacement (CTOD) test, and reduce the resistance to brittle fracture initiation.[4–8] Based upon these studies, some industry standards, such as API RP 2Z,[9] have been established, containing, in some form, a requirement that certain HAZ CTOD specimens must sample at least 15 pct of the coarse-grained HAZ (CGHAZ) microstructure. Meanwhile, steel manufacturers have been performing extensive research on LBZ phenomena in newly developed structural steel. Paradoxically, however, it is very interesting to note that LBZs have not been reported to be a significant cause of actual failure in practical welded structures, although many researchers have pointed out their deleterious influence on steel weldments. Related to that fact, some researchers have proposed that the conventional LBZ analysis based on a "crack-initiation prevention" approach may be too conservative, and that a "prevention of crack propagation" approach might be preferable, although there has been little experimental verification.[10]

The present work was undertaken to reveal the influence of LBZs on the fracture performance of QLT-9 pct Ni steel HAZs by an analysis of the crack-arrest behavior in an actual weld HAZ. First, simulated CGHAZ specimens were tested to confirm the presence of LBZs in the HAZ of this steel at cryogenic temperatures such as the LNG temperature, because, in general, the CGHAZ adjacent to the FL has the lowest toughness among various regions within the HAZ, due to unfavorable microstructures such as large prior grain size and martensite-austenite constituents. The distribution

JAE-IL JANG, Senior Researcher, Frontics, Inc., Research Institute of Advanced Materials, and BAIK-WOO LEE and JANG-BOG JU, Research Associates, and DONGIL KWON, Professor, School of Materials Science and Engineering, are with Seoul National University, Seoul 151-742, Korea. Contact e-mail: jijang@frontics.com WOO-SIK KIM, Principal Researcher, is with the Research and Development Center, Korea Gas Corporation, Ansan 425-150, Korea.

Manuscript submitted October 31, 2001.

Table I. Chemical Composition and Basic Mechanical Properties of QLT-9 Pct Ni Steel

Chemical Composition (Wt Pct)						Mechanical Properties at RT (at 77 K)		
C	Si	Mn	P	S	Ni	YP (MPa)	TS (MPa)	EL (Pct)
0.066	0.24	0.65	0.005	0.005	9.28	640 (910)	720 (1140)	36 (34)

Table II. Welding Conditions Used in This Study

Welding Method	Filler Metal	Polarity	Current (A)	Voltage (V)	Speed (cm/min)	Heat Input (kJ/cm)
SAW (flat)	Inconel type	DCEP	320 to 360	25 to 28	25–53	average 23
SMAW (vertical)	Hastelloy type	AC	100 to 130	20 to 40	6–20	average 28

of the LBZs near the FL was then examined using a microstructure-distribution map constructed from the actual HAZ specimens. Both compact crack arrest (CCA) tests and CTOD tests were conducted to evaluate the variations in crack-arrest toughness and crack-initiation toughness within the actual HAZs produced by the same welding processes as used during LNG storage tank construction. In addition, the LBZ effects on fracture resistance were examined by directly comparing the brittle-crack-arrest toughness (K_a) obtained from CCA tests with the brittle-crack-initiation toughness (K_c) calculated from CTOD test results. Although there have been many studies on LBZ phenomena or toughness variations in structural steel welds, few reports are available on the change in crack-arrest toughness within HAZs, and, furthermore, no systematic investigations have been made of the practical LBZ effects by directly comparing crack-arrest toughness and crack-initiation toughness.

II. EXPERIMENTAL PROCEDURES

A. *Material and Welding*

The 9 pct Ni steel used in this study was a commercial grade used for LNG storage tanks in Korea, whose chemical composition and basic mechanical properties are listed in Table I. The steel plates, which have a very low P and S content, were normally processed by the QLT heat treatment (Q: heated at 1093 K for 60 minutes, then quenched; L: heated at 963 K for 80 minutes, then quenched; and T: heated at 853 K for 60 minutes, then quenched.) Steel plates of 20 mm in thickness were machined into X-groove configurations and welded along the transverse-to-rolling direction by the shielded metal arc welding (SMAW) or submerged arc welding (SAW) processes. Welding was carried out under the same conditions as used during the construction of the tanks. Table II lists the welding parameters used during welding. Nondestructive X-ray examination found no significant defects in the completed weldments.

B. *Weld Simulations*

Weld simulations were performed to verify the distribution of LBZs within the HAZ of this steel. Oversized Charpy specimen blanks ($11 \times 11 \times 60$ mm) were thermally cycled in a metal thermal-cycle simulator. After reaching the first peak temperature (T_{P1}) of 1623 K concerning the CGHAZ, the specimens were cooled from 1073 to 773 K with the constant cooling times ($\Delta t_{8/5}$) of 13.5 and 19.4 seconds. The cooling rates were approximately equivalent to those of SAW and a SMAW, with heat inputs of 23 and 28 kJ/cm, respectively, in a 20-mm-thick plate.[11] These simulated welding conditions were based on the actual welding conditions listed in Table II. The peak temperature of the second weld thermal cycle (T_{P2}) varied between 1473 and 823 K. In order to view the microstructures of the simulated specimens in an optical microscope, 2 pct nital was used as a chemical etchant. The Charpy V-notch impact specimens were machined from the simulated specimen blanks and then tested at 77 K. The fracture surfaces of the specimens were also observed by scanning electron microscopy (SEM).

C. *Fracture-Toughness Tests Using Actual HAZ Specimens*

To assess the crack-arrest toughness, CCA tests were conducted at the LNG temperature of 111 K, in accordance with ASTM E1221.[12] The CCA test has many advantages over other crack-arrest-toughness testing methods, in its use of large-sized specimens: (1) the testing procedure has been standardized,[12] unlike most other crack-arrest tests; (2) the notch location within the HAZ can be easily selected by introducing a side groove in the CCA specimens; (3) unlike the double cantilever beam test using a similar-sized specimen, K_a can be evaluated in the CCA test even if $K_a > K_c$; and (4) this test, unlike other crack-arrest tests, can be conducted economically in the laboratory, since it does not require a testing machine with a large load capacity. Figure 1 is a schematic illustration of the CCA test setup and the specimen geometry. The electrodischarge-machined notches in the brittle bead in front of the side grooves were machined at various distances from the FL within the HAZ. The cross-sectional view in Figure 2 indicates the change in side-groove location (equivalent to notch location). Additionally, to measure crack-initiation toughness, the CTOD tests, which are generally used to evaluate the crack-initiation fracture toughness of steel weldments, were performed at 111 K, mainly in accordance with ASTM E1290 and BS 7448.[13,14] Figure 3 shows the testing arrangement and geometry of the CTOD specimen used in this study. The through-thickness precrack was also located at a distance from the FL. When calculating the CTOD values from the crack-mouth opening displacement data, the asymmetry of plastic deformation around the crack tip was taken into consideration; consequently, the "local CTOD" concept[15,16] was used, because the weldments had strength mismatches

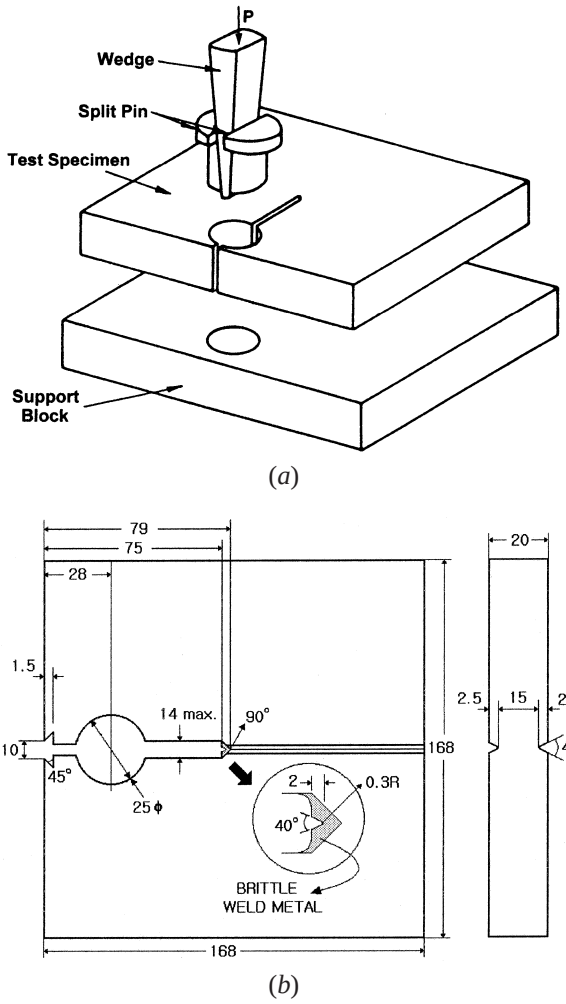

Fig. 1—Schematic views of (*a*) the setup for the CCA test and (*b*) the test specimen geometry.

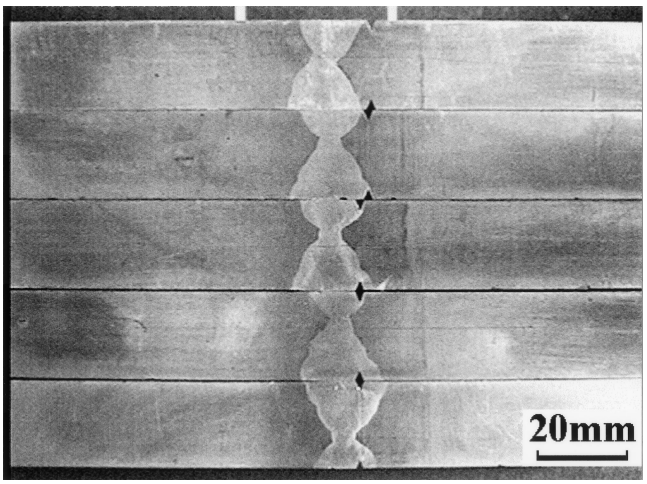

Fig. 2—Actual view of side-groove locations in CCA specimens.

between the austenitic weld metal and the ferritic base metal. In both the CCA and CTOD tests, at least three toughness values were obtained under each condition, and it was the smallest of these that was used to estimate the lower-bound toughness.

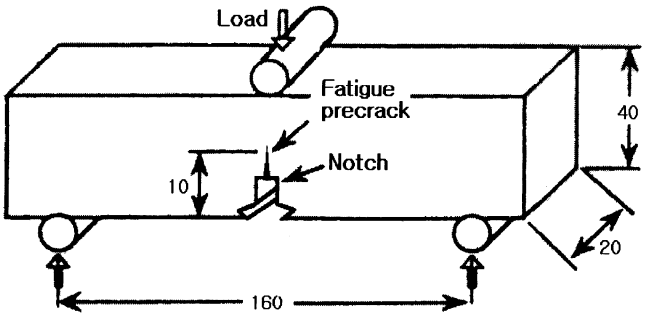

Fig. 3—Schematic illustration of CTOD test setup and specimen geometry.

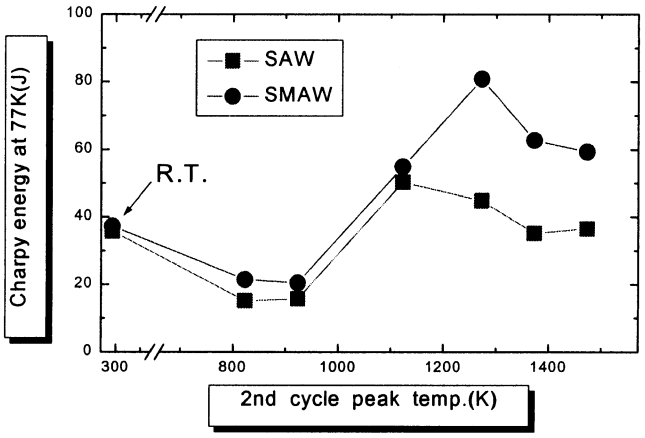

Fig. 4—Relation between Charpy impact energy at 77 K and the second peak temperature.

III. RESULTS AND DISCUSSION

A. *Determination of LBZs at Cryogenic Temperature*

Figure 4 shows the results of the Charpy impact tests, using simulated CGHAZ specimens at 77 K, as a function of the peak temperature of the second thermal cycle. Generally, the CGHAZ can be roughly divided into four characteristic zones, according to the peak temperature of the subsequent thermal cycle in a multipass welding procedure: (1) the unaltered (UA) CGHAZ, the region reheated above the specific temperature of grain growth or not reheated at all; (2) the supercritically reheated (SCR) CGHAZ, the region reheated above A_{C3}, (3) the intercritically reheated (IC) CGHAZ, the region reheated between A_{C1} and A_{C3}; and (4) the subcritically reheated (SC) CGHAZ, the region reheated below A_{C1}.[4–8] Among these, the SCR CGHAZ is often treated as fine-grained HAZ (FGHAZ) due to its recrystallized fine grain size.[17] In Figure 4, the second thermal cycles with peak temperatures between 1473 and 1373 K stimulate the UA CGHAZ, the cycles between 1273 and 1073 K simulate the SCR CGHAZ, and the cycles between 923 and 823 K simulated the IC CGHAZ. The SC CGHAZ was not considered in this study, because its properties were expected to be either similar to or superior to those of the UA CGHAZ, due to its low peak temperature and tempering effects. In both SMAW and SAW, the results exhibit low Charpy impact energies in two cases: the IC

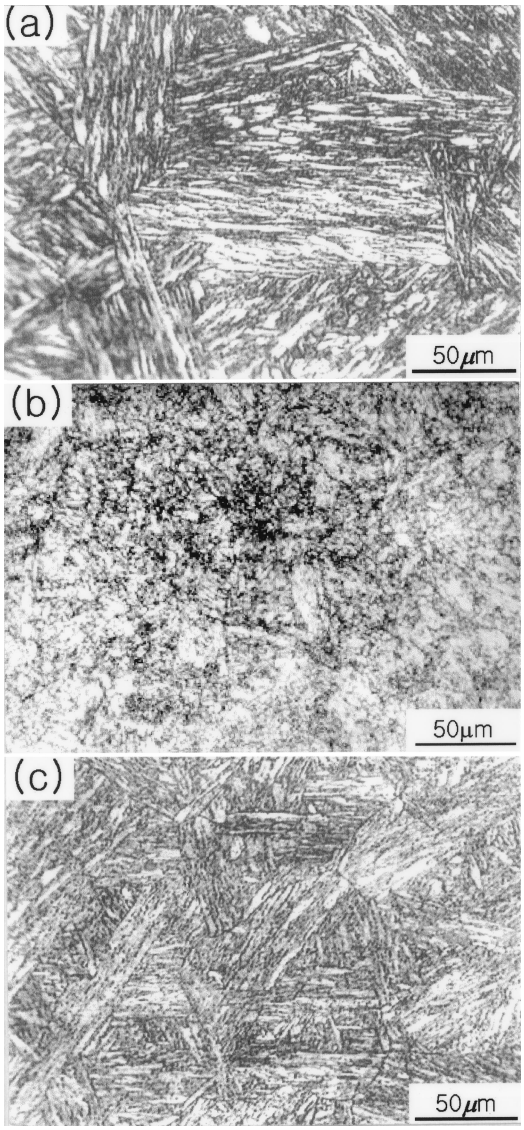

Fig. 5—Optical micrographs of (*a*) simulated UA CGHAZ, (*b*) simulated SCR CGHAZ, and (*c*) simulated IC CGHAZ.

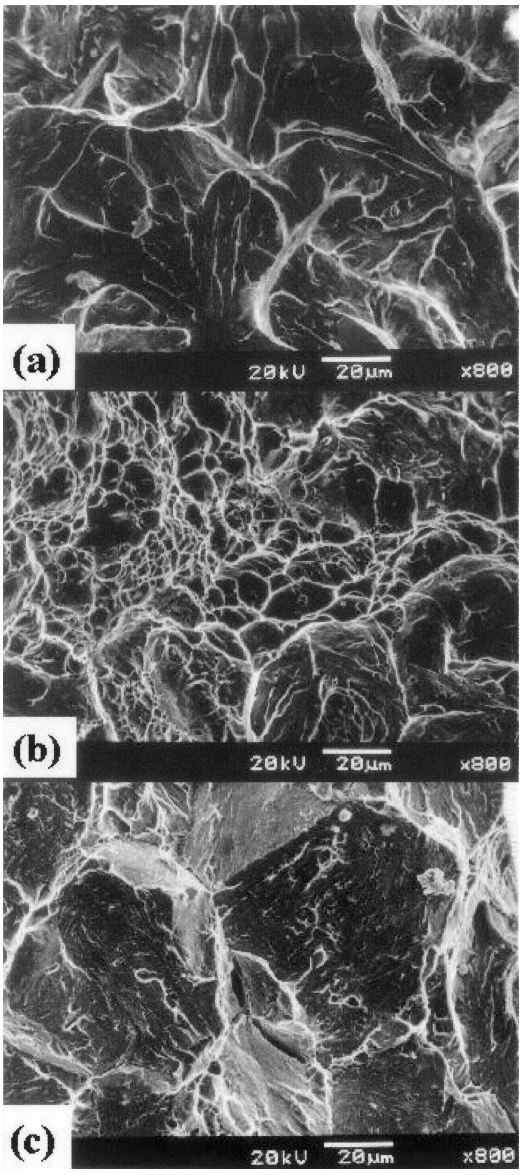

Fig. 6—SEM fractographs of Charpy tested specimens at 77 K: (*a*) simulated UA CGHAZ, (*b*) simulated SCR CGHAZ, and (*c*) simulated IC CGHAZ.

CGHAZ and UA CGHAZ. Otherwise, the specimens simulating the SCR CGHAZs show the highest value. The microstructures of the simulated CGHAZs were observed by optical microscopy. As shown in Figure 5, the UA and IC CGHAZs still consist of a coarsened microstructure of prior-austenite grains and martensite laths. On the other hand, the SCR CGHAZs have fine grains because, as mentioned earlier, the second thermal cycle above A_{C3} changes the coarse-grained microstructure to a fine-grained microstructure through recrystallization.[17] The fractographs of the specimens tested at 77 K in Figure 6 show clearly that the IC CGHAZ specimens fracture by an intergranular mode and the UA CGHAZ specimens fracture by a transgranular mode. On the other hand, the SCR CGHAZ specimens, with the highest impact value, fracture by the mixed mode of localized quasicleavage and mainly ductile dimple rupture. This change in fracture mode is consistent with the change in impact toughness. Consequently, it is possible to conjecture that the IC CGHAZ and UA CGHAZ might be the primary and secondary LBZs of QLT-9 pct Ni steel at cryogenic temperature.

B. *Microstructure-Distribution Map*

To verify the existence of the LBZs, a microstructure-distribution map of this steel HAZ was constructed. Maps of this sort are generally considered very useful for a systematic understanding of the relationship between fracture behavior and microstructure distributions within weld HAZs.[4,18,19] The representative microstructure-distribution map of the X-grooved weldment used in this study in Figure 7(a) was constructed from the macroetched weldment shown in Figure 7(b). The map was created by metallographic treatment of the weldment surface and by consideration of the thermal-cycle history. The thermal-cycle history is indicated based

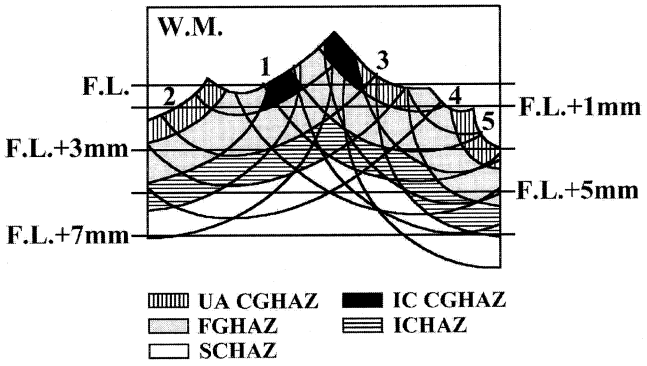

(*a*)

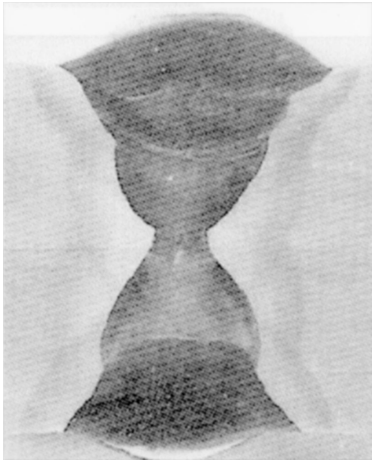

(*b*)

Fig. 7—Schematic views of (*a*) microstructure-distribution map for showing the change in fraction of subzones according to the notch locations, and (*b*) macroetched X-grooved HAZ used to construct (a).

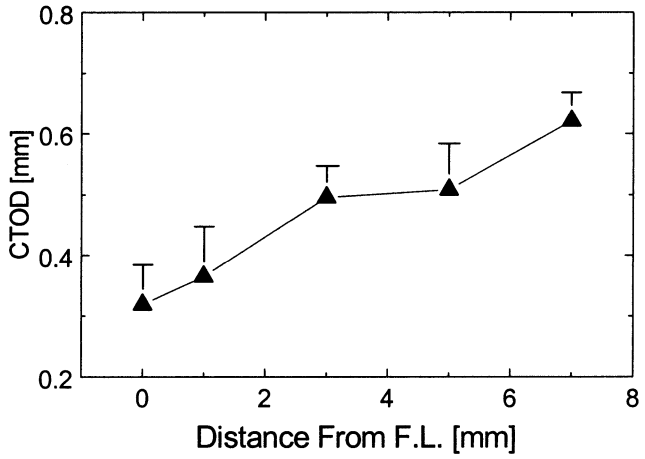

(*a*)

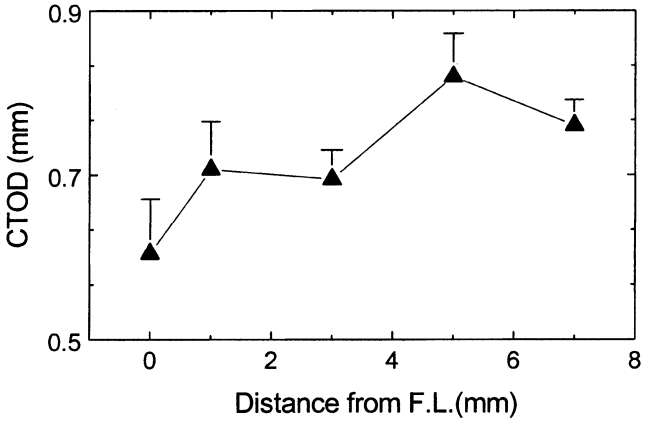

(*b*)

Fig. 8—Variations in CTOD values with distance from fusion line: (*a*) SMAW specimen and (*b*) SAW specimen.

on the macroetched weldment, using Eq. [1] for the thermal-cycle range according to peak temperature:[18,19]

$$\frac{r}{d_{\mathrm{HAZ}}} = \frac{\sqrt{(A_{C3} - T_0)}}{\sqrt{(T_p - T_0)}} \cdot \frac{\sqrt{(T_{mp} - T_0)} - \sqrt{(T_p - T_0)}}{\sqrt{(T_{mp} - T_0)} - \sqrt{(A_{C3} - T_0)}} \quad [1]$$

where r is the perpendicular distance from the fusion line to the region with peak temperature (T_P), T_{mp} is the melting temperature, T_0 is the interpass temperature, and d_{HAZ} is the distance between the FL and the HAZ line, observed by macroetching and taken as the A_{C3} boundary. In this study, A_{C3} is 968 K (obtained from a dilatometry test), T_{mp} is 1723 K, and T_0 is 383 K. In addition, 1323, 968, 823, and 723 K were used for T_P values of the CGHAZs, FGHAZs, intercritical (IC) HAZs with partially transformed microstructures, and subcritical (SC) HAZs with tempered microstructures, respectively. In the map, the line and the number indicate the notch location and welding sequence, respectively. It can be seen from the map that the microstructures of LBZs, *i.e.*, primarily the IC CGHAZ and secondarily the UA CGHAZ, are found mainly at the FL or FL + 1 mm.

C. *Change in Crack-Initiation and Crack-Arrest Toughness Within the Actual HAZ*

The results of CTOD tests for specimens that have undergone SAW and SMAW are shown in Figure 8. As expected, the crack-initiation toughness, *i.e.*, CTOD values, decrease as the precrack location approaches the FL from the base metal; this is attributable to the increase in the fraction of LBZs. However, even the regions near the FL such as the FL or FL + 1 mm, show moderate CTOD values, and there are no regions showing an abrupt decrease in fracture toughness. This result is interesting, because the regions near the FL have large fractions of IC CGHAZ and UA CGHAZ, these zones being defined as the LBZs of this steel's HAZ at cryogenic temperature. Additionally, the load-displacement curves obtained from the CTOD tests for the specimens with precracks located near the FL have many pop-ins, as shown in Figure 9: the specimen for the FL shows many pop-ins compared with that for the FL + 3 mm. One of the microstructural differences between the FL and FL + 3 mm is the presence of LBZs (IC CGHAZ and UA CGHAZ) in the former and their absence in the latter, and, thus, it can be conjectured that the pop-in behaviors are related to the existence of LBZs and to the crack-arrest behavior, as described subsequently.

The results of the CCA tests at 111 K are presented in

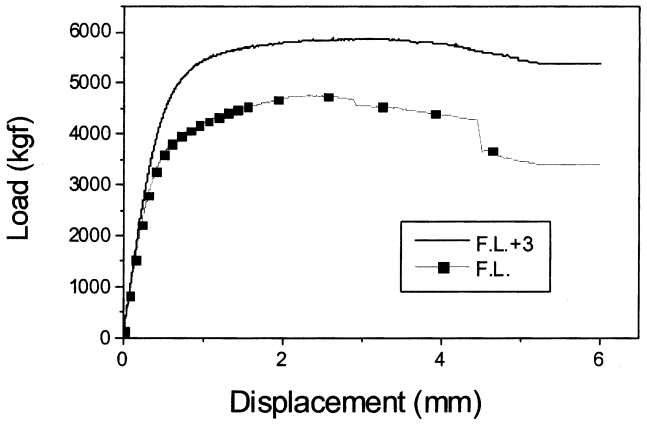

Fig. 9—Load-displacement curves obtained from CTOD tests using specimens precracked at fusion line (FL) and FL+3 mm, respectively.

Figure 10. Unlike the CTOD test results, the crack-arrest toughness values at the regions between the FL and FL + 3 mm are much higher than those at the FL + 5 mm and FL + 7 mm. These results are somewhat surprising because the regions near the FL have a larger LBZ fraction at their crack tips than the FL + 5 mm and FL + 7 mm regions, these latter two regions being expected to have almost exactly similar mechanical properties to the base metal because of the relatively low peak temperature of the welding thermal cycle. However, this result can be understood by considering the microstructure-distribution map in Figure 7. The main difference in microstructures between the high-arrestability regions and the other regions is not the existence of LBZs, but rather the large fraction of FGHAZs. By definition, FGHAZs have a very fine grain size due to recrystallization during welding, and this results in their increased toughness relative to the base metal. Malik *et al.*[10] have suggested that crack-arrest behavior is not a weakest-link-type event to be controlled by the most embrittled region such as LBZs, but rather a collective event that reflects the fracture toughness of the whole microstructure surrounding the crack-initiation point. In a similar light, a comparison of the CCA test results with the microstructure-distribution map clearly indicates that the high crack arrestability near the FL is controlled by the rule-of-mixtures of the microstructures at the crack-tip front of the CCA specimens and, thus, by the large fraction of FGHAZs irrespective of the presence of LBZs, although the fraction of LBZ at the FL and FL + 1 mm is large enough to initiate a brittle crack.

D. *Effects of LBZs on Fracture Resistance*

Direct comparison of brittle-crack-initiation toughness with brittle-crack-arrest toughness is one of the easiest ways to determine whether or not brittle facture has occurred. If K_c is higher than K_a and a brittle crack initiates, the crack cannot be arrested without propagation into a low-stress or high-temperature region. Conversely, if K_a is higher than K_c, the initiated brittle crack can easily be arrested. In this case, the associated pop-in behaviors can also be observed. So, the direct comparison of K_a with K_c is very effective in predicting the practical risk level associated with an LBZ.

For direct comparison, the thickness difference between

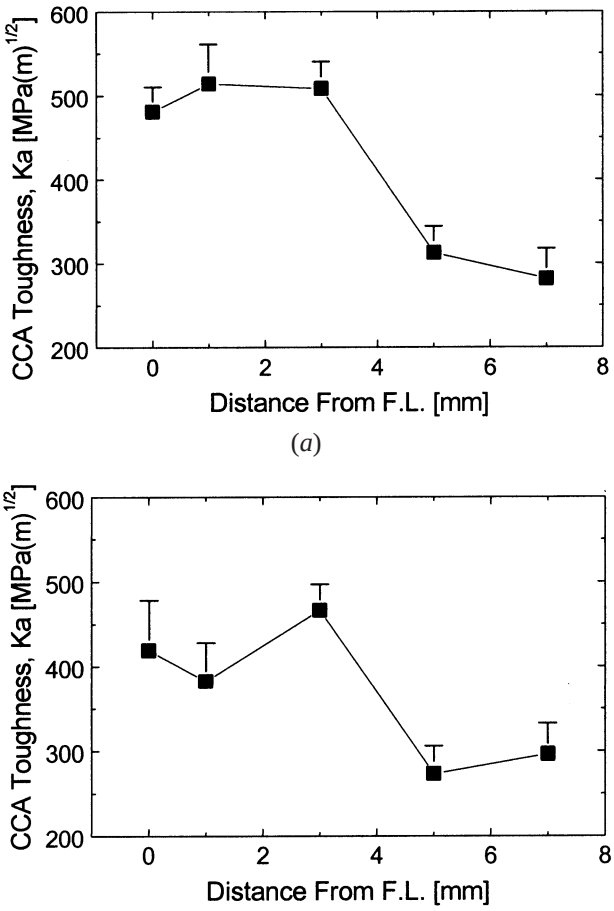

Fig. 10—Variations in crack arrestability along the distance from fusion line: (*a*) SMAW specimen and (*b*) SAW specimens.

the 20-mm-thick CTOD specimens and the CCA specimens of the same thickness but featuring 5-mm-deep side grooves should first be considered, since fracture toughness increases with decreasing thickness. The Japanese standard WES-3003[20] reports the following correction method for K_a, in accordance with the thickness change for steels used at low temperature, like the 9 pct Ni steel:

$$f(B) = 1 - \frac{1}{20}(B - 30) \qquad [2a]$$

$$K_a(B_1) = K_a(B_2) \cdot \frac{f(B_1)}{f(B_2)} \qquad [2b]$$

where B is the specimen thickness in millimeters, and $K_a(B)$ is the K_a value of the specimen with a thickness of B. Machida *et al.*[21] applied this equation to a QT-treated 9 pct Ni steel and reported that they could successfully predict the toughness of a specimen with other thicknesses. Similarly, here, the crack-arrest-toughness values obtained from the specimens with side grooves were corrected by the correction ratio $f(20)/f(15) = 1.5/1.75$. Figure 11 shows the thickness-corrected value of K_a.

Next, the brittle-crack-initiation toughness, represented by K_c, must be extracted from the CTOD toughness. Generally, CTOD can be expressed by

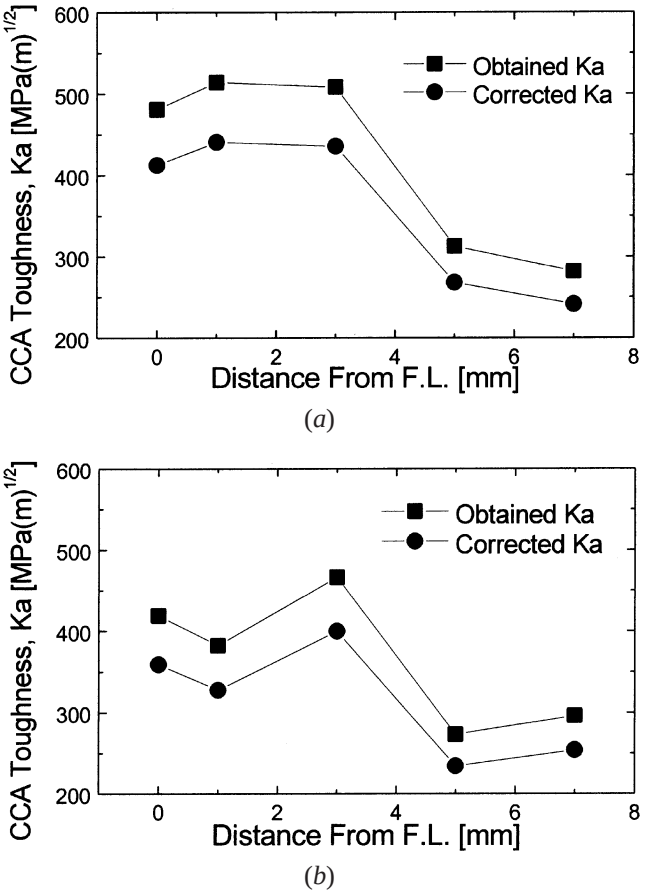

Fig. 11—Correction of thickness reduction due to side-groove in CCA specimen: (*a*) SMAW specimen and (*b*) SAW specimen.

$$\delta = \delta_{el} + \delta_{pl} = \frac{K^2(1-\nu^2)}{m\sigma_{YS}E} + \frac{r_p(W-a)}{r_p(W-a)+a} V_g \qquad [3]$$

where δ_{el} and δ_{pl} are the elastic and the plastic terms of the CTOD, respectively, and other symbols are the standard notation in ASTM E1290.[13] Thus, Eq. [4] has been used for the conversion of CTOD to K.[10,21]

$$K^2 = m\sigma_{YS}E(\delta_{el}) \qquad [4]$$

where m is a dimensionless constant that is approximately 1 for a plane-stress condition and approximately 2 for a plane-strain condition, and σ_{YS} and E are the yield strength and elastic modulus, respectively. The measured CTOD toughness in Figure 8 is the sum of δ_{el} and δ_{pl}, and, thus, δ_{el} should be extracted from the measured CTOD value (δ_{measured}) to predict K_c. Since it is not easy to estimate the exact ratio of δ_{el}/δ_{pl}, various ratios of δ_{el}/δ_{pl} are assumed in this study.

Figure 12 shows a direct comparison between the thickness-corrected value of K_a and the converted K_c value using various ratios of δ_{el}/δ_{pl}. The converted K_c value decreases with decreasing ratio of δ_{el}/δ_{pl}. In the figure, δ_{el} can be assumed to be equal to δ_{measured} only when the obtained CTOD is the critical CTOD (δ_C), *i.e.*, δ_{pl} is almost negligible. However, the case is not applicable in this study, because the obtained maximum CTOD (δ_m) includes both δ_{el} and δ_{pl}, which are in the relationship $\delta_{el} < \delta_{pl}$, as shown in Figure 9. So, it can be predicted that the actual K_c value is

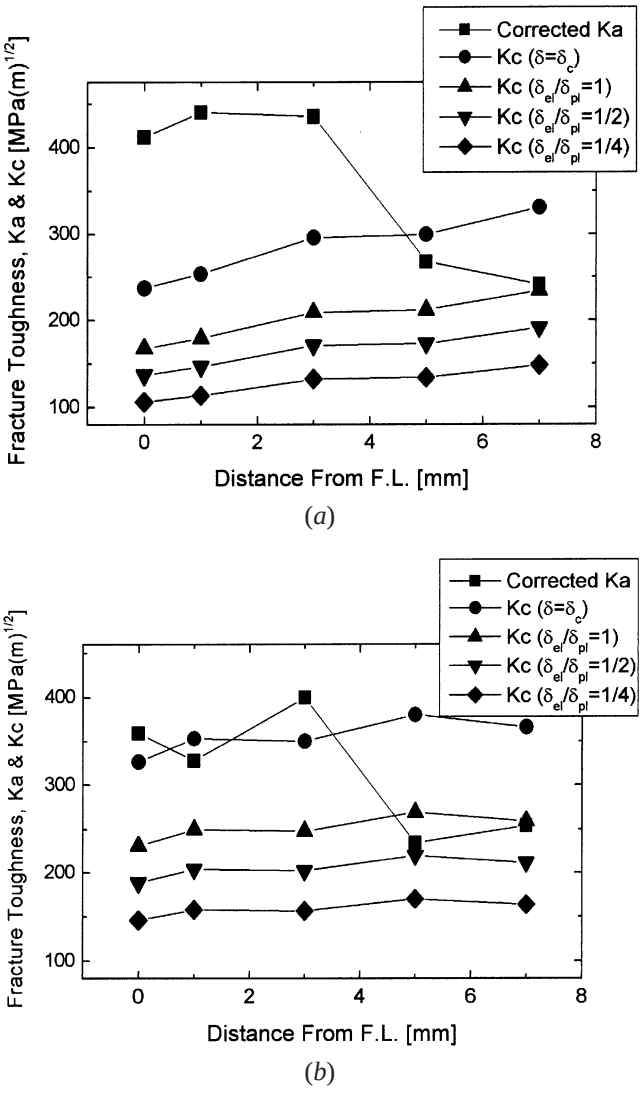

Fig. 12—Comparison of corrected K_a with K_c as calculated by Eq. [5]: (*a*) SMAW specimen and (*b*) SAW specimen.

lower than the K_c value converted by the assumption of $\delta_{el}/\delta_{pl} = 1$. Ray *et al.*[22] have reported that the ratio of δ_{el}/δ_{pl} in tough HY-80 steel is approximately 0.25. Based upon the previous consideration, we see in Figure 12 that the K_a values of the HAZs are higher than the K_c ones, which are converted in a reasonable way. In particular, K_a is much higher than K_c near the FL, where LBZs are mainly located. Even in the unacceptable case of $\delta_{el} = \delta_{\text{measured}}$, the K_a value of the HAZs is much higher than K_c in SMAW specimens and is similar to K_c in SAW specimens. Therefore, it is apparent that even if a brittle crack initiates at (or near) LBZs, it will be easily arrested after only a short propagation distance.

The crack-arrest behavior is shown schematically in Figure 13. When there is a through-thickness crack near the FL, the LBZs exist in the form of a continuous band along the direction of crack propagation. In this case, maintenance of a crack front through the thickness and continued propagation depend on the toughness of the material adjacent to the LBZs as well the LBZs themselves, indicating that, for crack propagation featuring a uniform shape, the microstructures surrounding the LBZs should have similar toughness to the

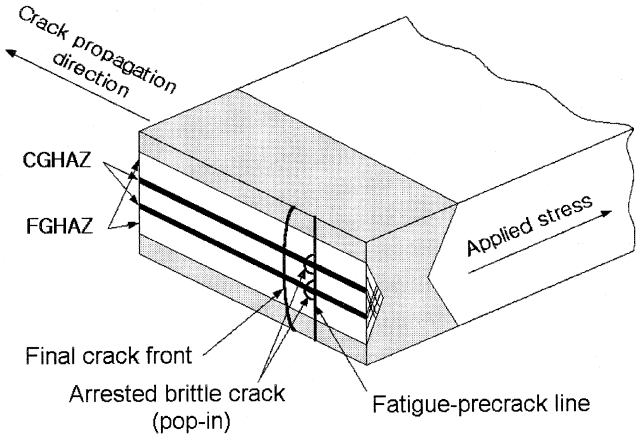

Fig. 13—Schematic illustration of a crack front following LBZs.

LBZs themselves. But, the regions including the FGHAZ have much higher toughness than the LBZs, and these regions suppress the propagation of a brittle crack. Therefore, the initiated crack is arrested after a short propagation distance. This crack-arrest behavior can be verified by the presence of pop-ins in the load-displacement curve obtained from the CTOD tests, as shown in Figure 8. These pop-ins are generally allowable and are not thought to affect the integrity of the welded structures. Thus, this investigation has determined that in regard to crack-arrest behavior, LBZs of the QLT-9 pct Ni steel may not limit the practical safety performance of the practical weldments in LNG storage tanks. The results also suggest that the conventional concept of LBZ effects based on crack-initiation behavior may be overconservative.

IV. CONCLUSIONS

The practical influence of LBZs on the fracture resistance of the QLT-9 pct Ni steel HAZ was investigated by comparing the crack-initiation toughness with the crack-arrest toughness obtained from CTOD and CCA tests, respectively. The primary results of this investigation are as follows.

1. The results of Charpy impact tests using the simulated CGHAZ specimens show that IC CGHAZ and UA CGHAZ are the primary and secondary LBZs, respectively, of the steel at the cryogenic temperature at which 9 pct Ni steel is generally used.
2. The change in crack-initiation toughness within the HAZ was evaluated by CTOD tests using welded HAZ specimens. Although the CTOD values decrease approaching the FL, the values at all the regions show moderate toughness. Instead, many pop-ins were observed in the load-displacement curves from the CTOD tests for the specimens with precracks near the FL.
3. Crack-arrest toughness was measured at various distances from the FL by the CCA tests. Unlike CTOD test results, the regions near the FL showed high arrest-toughness values in spite of the presence of LBZs. This is mainly because the crack-arrest behaviors are rule-of-mixtures-type events controlled by various microstructures surrounding crack-initiation points, while the crack-initiation behaviors are weakest-link-type events controlled by the most brittle microstructures, such as the LBZ.
4. By comparing the brittle-crack-arrest toughness (K_a) with the brittle-crack-initiation toughness (K_c), it is found that K_a is much higher than the K_c value converted from the CTOD value at the regions near the FL, where the LBZ mainly exists. Therefore, a brittle crack initiating in the LBZ is expected to be arrested after propagating a very short distance. This arrest behavior is also verified by the pop-in phenomenon observed in CTOD tests. It can be concluded that the LBZ of the QLT-9 pct Ni steel is not a critical risk factor in the safety of actual weld joints in LNG storage tanks, from the viewpoint of crack-arrest behavior.

ACKNOWLEDGMENTS

The authors are very grateful to Professor Masao Toyoda, Osaka University, for his helpful discussion of this work.

REFERENCES

1. C.H. Lee, S.W. Lee, J.Y. Yoo, and W.Y. Choo: *Proc. 2nd Pacific Rim Int. Conf. on Advanced Materials and Processing*, Kyongju, Korea, 1995, pp. 2035-44.
2. J.-B. Lee and J.-K. Han: *J. Kor. Weld. Soc.*, 1995, vol. 13, pp. 34-40.
3. J.I. Kim, C.K. Syn, and J.W. Morris, Jr.: *Metall. Trans. A*, 1983, vol. 7A, pp. 93-103.
4. D.P. Fairchild: *Fatigue and Fracture Testing of Weldments*, ASTM STP 1058, ASTM, Philadelphia, PA, 1990, pp. 117-41.
5. B.C. Kim, S. Lee, N.J. Kim, and D.Y. Lee: *Metall. Trans. A*, 1991, vol. 22A, pp. 139-49.
6. S. Lee, B.C. Kim, and D. Kwon: *Metall. Trans. A*, 1992, vol. 23A, pp. 2803-16.
7. M. Toyoda: *J. Jpn. Weld. Soc.*, 1993, vol. 62, pp. 603-16.
8. C.L. Davis and J.E. King: *Metall. Mater. Trans. A*, 1994, vol. 25A, pp. 563-73.
9. API RP 2Z, 2nd edition, *Recommended Practice for Preproduction Qualification for Steel Plates for Offshore Structures*, American Petroleum Institute, Washington, D.C., 1992.
10. L. Malik, L.N. Pussegoda, B.A. Gravile, and W.R. Tyson: *J. OMAE (Trans. ASME)*, 1996, vol. 118, pp. 292-99.
11. K. Masubuchi: *Analysis of Welded Structures*, Pergamon Press, New York, NY, 1980, ch. 2.
12. *Standard Test Method for Determining Plane-Strain Crack Arrest Fracture Toughness, K_{Ia}, of Ferritic Steel*, ASTM Standard E 1221, ASTM, Philadelphia, PA, 1988.
13. *Standard Test Method for Crack-Tip Opening Displacement (CTOD) Fracture Toughness Measurement*, ASTM Standard E 1290, ASTM, Philadelphia, PA, 1993.
14. *Fracture Mechanics Toughness Tests, Part 2: Method for Determination of K_{IC}, Critical CTOD and Critical J Values of Welds in Metallic Materials*, British Standard 7448, British Standards Institution, London, UK, 1997.
15. K. Satoh, M. Toyoda, F. Minami, S. Satoh, M. Nakanishi, and K. Arimochi: *J. Jpn. Weld. Soc.*, 1983, vol. 52, pp. 154-61.
16. J.-I. Jang, Y.-C. Yang, W.-S. Kim, and D. Kwon: *Adv. Cryog. Eng.*, 1998, vol. 44, pp. 41-48.
17. F. Minami, M. Toyoda, C. Thaulow, and M. Hauge: *Q. J. Jpn. Weld. Soc.*, 1995, vol. 13, pp. 508-17.
18. Y. Nakao, H. Oshige, and S. Noi: *Q. J. Jpn. Weld. Soc.*, 1985, vol. 3, pp. 766-73.
19. S. Suzuki, K. Bessyo, M. Toyoda, and F. Minami: *Q. J. Jpn. Weld. Soc.*, 1995, vol. 13, pp. 302-08.
20. *Evaluation Criterion of Rolled Steels Used for Low Temperature Application*, WES Standard 3003, Japan Welding Engineering Society, Tokyo, Japan, 1983.
21. S. Machida, N. Ishikura, N. Kubo, N. Katayama, Y. Hagiwara, and K. Arimochi: *J. High Pressure Inst. Jpn.*, 1991, vol. 29, pp. 25-39.
22. K.K. Ray, S. Roy, A. Bhaduri, and S. Ray: *Int. J. Fracture*, 1995, vol. 70, pp. R3-R8.